

## INVESTIGATIONS INTO THE HIGH TEMPERATURE BEHAVIOUR OF UNSTABILISED RAMMED EARTH

Christopher Beckett<sup>1</sup>, Kyriacos Kazamias<sup>2</sup> and Angus Law<sup>1</sup>

<sup>1</sup> School of Engineering, The University of Edinburgh, [christopher.beckett@ed.ac.uk](mailto:christopher.beckett@ed.ac.uk)

<sup>2</sup> FEC International, United Kingdom, [kazamiasedin@gmail.com](mailto:kazamiasedin@gmail.com)

### ABSTRACT

The thermomechanical properties of earthen construction materials are relatively unknown: particularly under the temperatures associated with fire exposure. This paper presents an exploratory study examining the transient thermal behaviour of unstabilised rammed earth samples exposed to controlled, unidirectional incident heat fluxes of 20, 35 and 50 kW/m<sup>2</sup>, reaching temperatures of approximately 500°C. Temperatures throughout the samples were recorded using embedded thermocouples. Results demonstrated the loss of mechanical water at 100°C and subsequent oxidation of the exposed sample surfaces to depths between 5 and 10 mm. Inverse heat transfer modelling was used to estimate effective material thermal properties for the samples and the limitations of this approach are discussed.

**Keywords:** Rammed earth; fire; thermal performance; thermal modelling.

### INTRODUCTION

Scientific scholarship on earthen construction materials over the past two decades has demonstrated the critical relevance of hygroscopy to governing earthen materials' mechanical and thermal performance. Hydro-mechanical properties manifest due to suction forces between soil aggregates; capillary water forms concave menisci between hydrophilic aggregates, producing a net tensile force which draws those aggregates together (Jaquin *et al.*, 2009; Zhou *et al.*, 2016; Beckett *et al.*, 2018). Similarly, hygrothermal properties arise as the material absorbs or releases moisture, which acts to vary thermal properties and regulate internal humidity (Adam and Jones, 1995; Hall and Allinson, 2009; Arrigoni *et al.*, 2017).

Both hydro-mechanical and hygrothermal properties are functions of the amount and distribution of capillary water held within the material pore spaces and so could be considered aspects of more general thermo-hydro-mechanical behaviour (Gens, 1997). However, to date, thermo-hydro-mechanical properties have only been examined for temperatures up to 100°C, as these conditions are the most relevant to geotechnical engineering (Gens, 2010). Few works have examined the performance of earthen materials under temperatures associated with fire exposure (i.e. far exceeding 100°C)

and none from a thermo-hydro-mechanical perspective. How material properties might vary under these conditions is, therefore, unknown. A parallel can be drawn, however, between earthen materials exposed to extreme temperatures and clay bricks undergoing firing in a kiln. Brickmaking uses clayey soils (i.e. mixtures of clay minerals, silts and some sand) as a raw material, i.e. similar material to the fine fraction comprising a rammed earth mix. Principal hydraulic and thermo-chemo-dynamic processes during firing are shown in Figure 1 and summarised in Table 1; temperature ranges vary per material but those given are approximate for kaolinitic clays (the reader is referred to Johari et al. (2010) and Akinshipe and Kornelius (2017) for

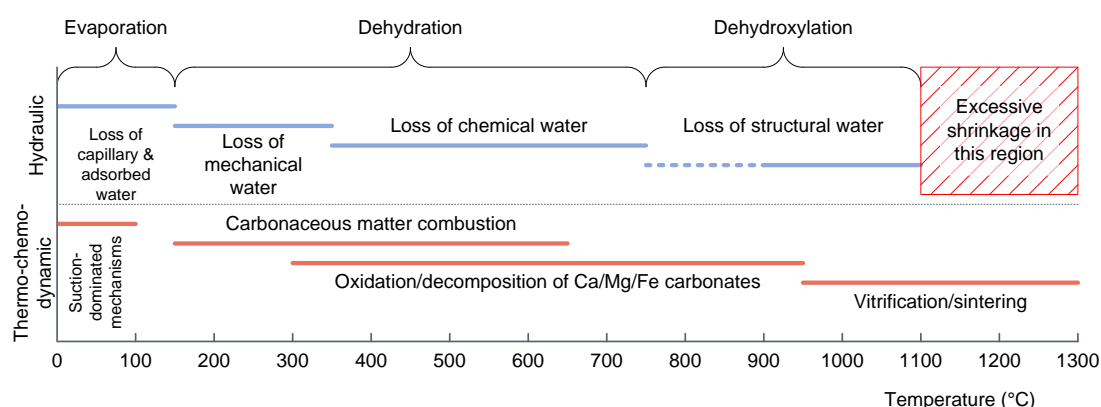


Figure 1. Key hydraulic and thermo-chemo-dynamic processes and associated temperature ranges during typical clay brick firing

Table 1. Hydraulic and thermo-chemo-dynamic processes associated with clay brick firing

Hydraulic processes	<i>Evaporation</i> : temperatures are sufficient to remove pore water menisci suspended between soil particles.
	<i>Dehydration</i> : removal of water that is chemically bonded to the clay particles. Here, the process is separated into loss of mechanical water, being that which is loosely bound to the particles or adsorbed between platelet stacks, and chemical water, being that which is part of the hydrous clay minerals.
	<i>Dehydroxylation</i> : removal of hydroxyl ions from clay crystal structure
Thermo-chemo-dynamic processes	<i>Suction-dominated</i> : changes in pore water pressure due to moisture migration result in material shrinkage and aggregate rearrangement (Beckett and Augarde, 2013).
	<i>Carbonaceous matter combustion</i> : breaking down of the carbonaceous matter and carbonates forming hydrocarbons and carbonaceous residue.
	<i>Oxidation</i> : carbonates of Ca, Mg and Fe thermally decompose into their oxides, producing carbon dioxide and/or monoxide, depending on the oxygen availability within the kiln.
	<i>Vitrification/sintering</i> : clay materials partially melt and coat the remaining solid particles, bonding them together and developing the fired brick's strength.

detailed discussion on these processes). These processes indicate that capillary water could readily be assumed to have evaporated under conditions associated with fires (Mielenz et al., 1953). Loss of capillary water commensurately suggests a loss of material integrity, owing to the loss of suction: a catastrophic scenario for structures expected to survive or provide protection during fires. This work therefore examines the performance of unstabilised rammed earth specimens subjected to high temperatures via a constant heat flux, to explore methods to predict thermal property evolution and provide insight into material transient thermal behaviour under these conditions.

## **EXPERIMENTAL PROGRAMME**

### **Materials**

Earthen construction has been popular for millennia due to its use of locally available material. However, natural soils are highly variable and so introduce additional complications during laboratory testing. Here, an artificial soil was manufactured from constituent silty clay (Birtley Clay, PL 25%, LL 57%, 50% kaolinitic clay by mass) and fine, medium and coarse silica sand fractions to permit greater control over the particle grading (Hall and Djerbib, 2004). Constituent materials were combined to produce a well-graded material of approximately 70% sand and 30% silty clay, following recommendations from Houben and Guillaud (1994) for rammed earth materials. Rammed earth was chosen here, as opposed to other popular earthen construction techniques, as the method lends itself well to instrumentation via embedded sensors (discussed in subsequent sections). Particle grading curves for the constituent materials and combined mix are shown in Figure 2. It is acknowledged that rammed earth soils commonly include gravel-sized particles (>2mm); such particles were not included here, however, to avoid compaction issues and damage to sample instrumentation (again, as discussed in the following sections). As such, the coarsest particle content marginally falls outwith the recommended grading limits. It is further noted that particle size distribution alone is not a reliable indicator of material suitability or likely behaviour. However, an understanding of the engineered mix's mineralogy, texture and compaction conditions will permit a qualitative extension of results to other mixes and materials.

Compaction testing was performed according to the BS 1377-4:1990 heavy manual compaction test, with the exception that a drop height of 300 mm was used instead of 450 mm; the reduced height reduces the compaction energy and produces material dry densities closer to those created *in situ* (Smith and Augarde, 2014). The maximum dry density and optimum water content (OWC) for this combination were 2070 kg/m<sup>3</sup> and 7.5% respectively.

### **Specimen Instrumentation and Preparation**

100mm cube specimens were manufactured for testing; although cylindrical specimens are more common for geotechnical analyses, cubes facilitate specimen alignment within the heating apparatus.

Nine type-K fiberglass shielded thermocouples were placed at nominal 10 mm intervals along the specimen vertical centreline to examine thermal changes

throughout the material during heating. 10 mm intervals were selected to provide some granularity for thermal property modelling. Thermocouples were installed by compacting a 10 mm deep layer and placing the thermocouple upon it, passing through the mould wall via pre-drilled ports as shown in Figure 3. This process was repeated until the specimen reached the required height. For each layer, a known mass of material (wetted to the OWC) was compacted to a controlled volume to create a layer of density equal to the maximum identified through compaction testing (e.g. following Beckett et al., 2018). Previous work (Beckett and Ciancio, 2014) demonstrated that embedding thermocouples in this manner creates a good thermal contact between the sensor and the surrounding material. The compaction process, however, introduced potential errors with respect to the placement of the thermocouples as it is possible that they may have become displaced during the fabrication; this will be discussed further below.

Once manufactured, specimens were removed from the mould and left to dry to constant mass under ambient conditions (relative humidity – RH –  $50\pm 10\%$  and temperature  $15\pm 5^\circ\text{C}$ ) for 7 days. All specimens were exposed to the same ambient conditions to impose approximately consistent internal water contents (approximately 4% by mass) prior to thermal testing.

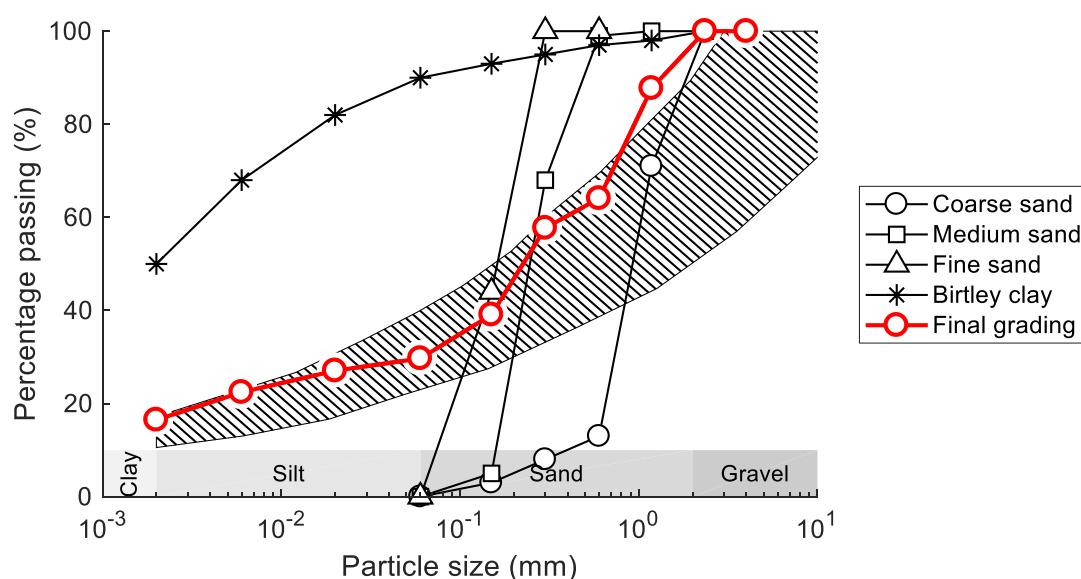


Figure 2. Raw material and final particle grading curves for engineered rammed earth soil, with recommended grading limits (hatched region, Houben and Guillaud, 1994)

### Heating

The specimens were heated with a cone heater (BS ISO 5660-1:2015), capable of controlling the incident radiative flux on the surface of the material. Specimens were exposed to incident heat fluxes of 20, 35 and 50 kW/m<sup>2</sup> for a duration of one hour in the vertical horizontal orientation (i.e. heated from above). Specimen sides were wrapped in ceramic wool to minimise lateral losses from the sample (and therefore

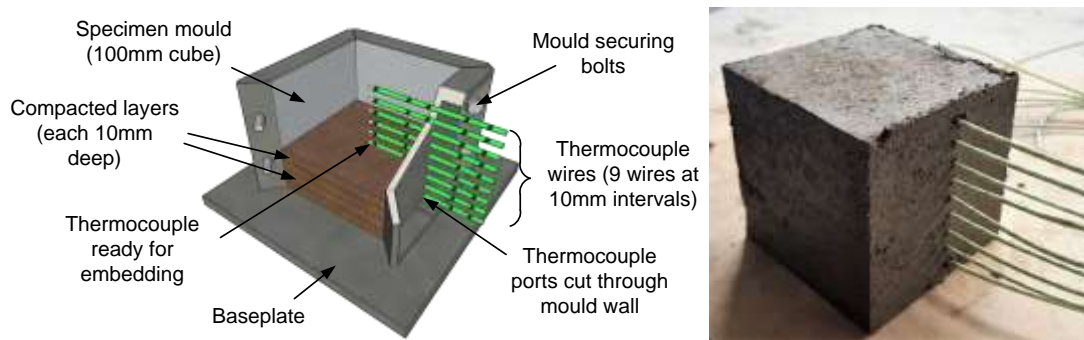


Figure 3. Schematic cutaway showing specimen manufacture: layer compaction and thermocouple placement. Some mould features not shown for clarity. Thermocouple positions are indicative: thermocouples were installed incrementally per compacted layer. Final compacted specimen shown on the right.

more readily approximate a one-dimensional heat transfer condition). Exposed thermocouple wires were also wrapped in thermal wool when in proximity to the heater to prevent damage. Temperatures were recorded at a rate of 1 Hz by means of an external logger. After testing, specimens were cut down their vertical centreline (using a diamond saw) to expose the thermocouple tips and so determine their true location and proximity to the heated surface. Three specimens were tested per incident heat flux (nine specimens in total).

### Thermal Property Modelling

The thermal properties of the specimens were estimated using an inverse heat transfer analysis based on a Crank-Nicholson finite difference scheme. To avoid uncertainties associated with estimating the convective heat transfer coefficient ( $h$ ) and emissivity on the surface of the sample ( $\epsilon$ ), the readings from the front and rear embedded thermocouples were used to define the thermal boundary conditions as functions of time and temperature only. Consequently, the only unknowns were the constituents of the thermal diffusivity ( $\alpha$ ) – that is conductivity ( $k$ ), specific heat capacity ( $c_p$ ), and bulk density ( $\rho$ ). For computational simplicity, it was assumed that the spacing of the finite difference nodes was equal at 1 mm; the spacing allowed the results of the model to be compared to the measured data for the location in which the thermocouple was found to be placed (to an accuracy of 1 mm).

### Thermal Property Reference Values and Limits

The presence of water within the sample introduces a heat sink term associated to the phase change of the water. This can be represented by either adding an additional heat sink term into the energy equation, or by using apparent thermal properties wherein the values of  $k$ ,  $\rho$  and  $c_p$  are adjusted to accommodate the latent heat of vaporisation for temperatures around 100°C. The latter approach is commonly used by those within the structural fire engineering community for heat transfer modelling in concrete. This approach was adopted in this paper to determine the feasibility of using apparent material properties for heat transfer modelling in rammed earth. Temperature

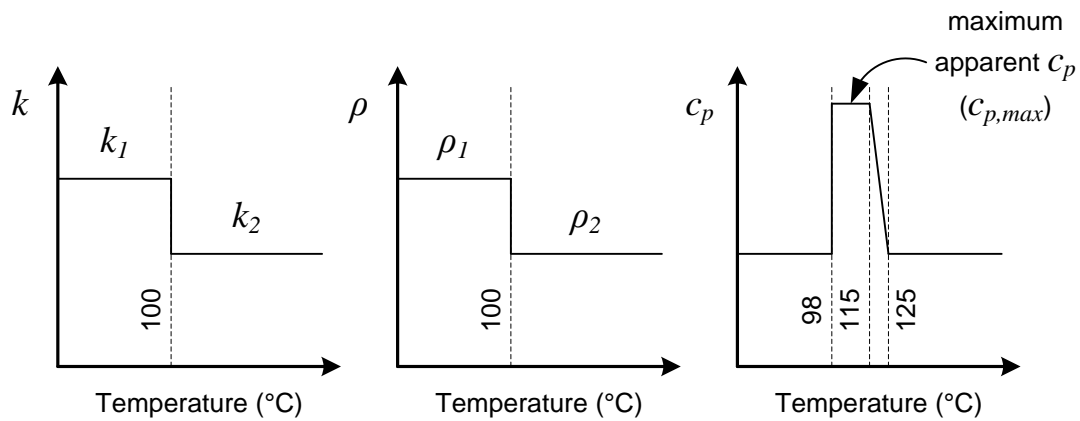


Figure 4. Temperature thresholds for varying apparent thermal property values: thermal conductivity ( $k$ ); bulk density ( $\rho$ ); and specific heat capacity ( $c_p$ )

thresholds used to vary the parameters are shown schematically in Figure 4. The various thermal properties of interest were defined as independent variables and a Levenberg-Marquardt algorithm was used to identify the optimal values that gave the best match to the recorded data. This scheme was implemented in MATLAB using the pre-existing toolbox function and followed the approach described by Hidalgo (2015).

The optimisation method requires bounds to be set on the maximum and minimum values for each independent variable. These values were set based on a review of previous literature. Hall and Allinson (2009) examined rammed earth thermal property variation between wet and dry conditions for a 70% sand and 30% silty clay mix. They found that thermal conductivity was around 1.8 W/mK for a saturated material and roughly 0.8 W/mK when dry. Given this evidence about varying conductivity between dry and wet samples, it was decided to use two different values of  $k$  – one below 100°C ( $k_1$ ) and one above 100°C ( $k_2$ ). It is noted, however, that Hall and Allinson's values were for cement-stabilised rammed earth (6% Ordinary Portland Cement by mass of dry soil, necessary to maintain an intact sample whilst saturated). Little work has been done to examine cement's role in establishing the thermal properties of natural (or here, engineered) soils. However, testing on crushed limestone suggests that cement may affect microstructure formation, and so, by extension, thermal properties (Beckett and Ciancio, 2014). Upper and lower bounds of 2.0 and 0.5 W/mK were therefore selected for thermal parameter estimation to accommodate uncertainty surrounding aggregation behaviour.

The density of each of the specimens was carefully controlled during manufacture. Hence, bulk density at testing was used for densities below 100°C ( $\rho_1$ ) and the material dry density thereafter ( $\rho_2$ ).

Little work has examined specific heat capacities of earthen materials, owing to the transient nature of the required tests. However, values from Hall and Allinson would suggest that these were around 850 J/kgK. As a consequence, the minimum and maximum bounding values for specific heat capacity were set to at 750 J/kgK and 950 J/kgK respectively. In addition to the specific heat capacity of the material, the

latent heat of the water was represented using an apparent maximum  $c_p$  ( $c_{p,max}$ ) which had a maximum value at around 100°C, following the approach of BS EN 1992-1-2:2004. The shape of this function was selected to peak at a constant between 98°C and 115°C; a linearly descending branch was implemented returning to the original  $c_p$  at 125°C (Figure 4). This final assumption with respect to apparent specific heat capacity introduces a number of limitations into the model that will be discussed below.

## RESULTS AND DISCUSSION

### Heating response

Example thermocouple data captured during heating is shown in Figure 5, demonstrating the penetration of heat through the specimens. Each dataset shows a plateau at 100°C which is characteristic of the presence (and phase change) of water within the material.

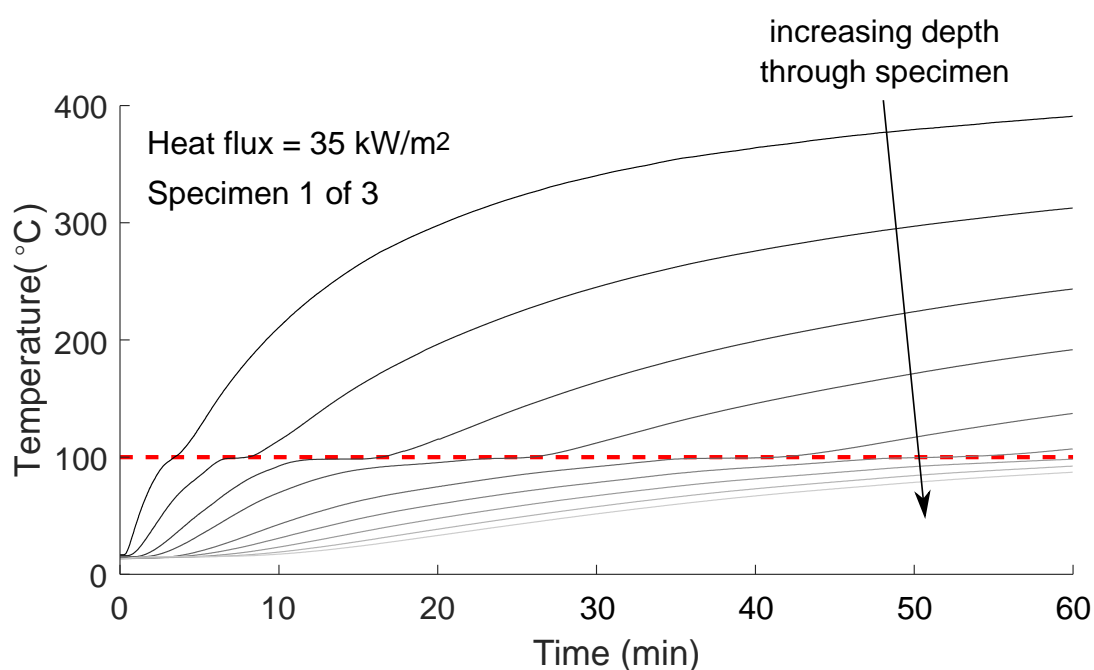


Figure 5. Example specimen temperature changes during heating; dashed line shows the boiling point of water at 100°C (specimen tested at 35 kW/m<sup>2</sup>)

The physical condition of the sample was notable because, although capillary water was ostensibly removed, all specimens remained intact throughout (and after) the test. It is possible that this was a consequence of no external load being applied to the specimens; under loading, material lacking capillary water may fail. Figure 6 shows a typical section through one of the specimens after heating. All specimens displayed a reddening of the material closest to the heater, to a depth of roughly 5 mm, preceded by roughly 10 mm of darkened material; the remaining material was seemingly unmodified. Material discolouration nearest the heat source suggests that calcium,

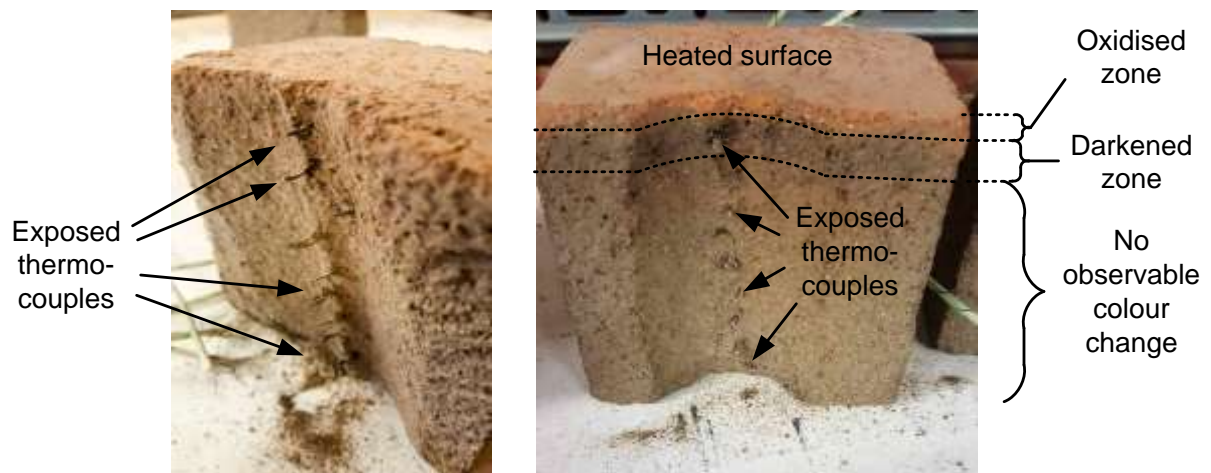


Figure 6. Example cross section of tested specimen showing exposed thermocouples (specimen tested at 50 kW/m<sup>2</sup>)

magnesium and iron carbonates in the clay had begun to oxidise (Johari et al., 2010). Discolouration in the darkened region below the (supposed) oxidized layer (where temperature reached around 400°C) may have been due to dehydration of water chemically bound to the clay particles and combustion of carbonaceous material: a process which occurs in kaolin clays at temperatures above 350°C (Johari et al., 2010). Goodman et al. (2018) examined microstructural changes in kaolinitic clays exposed to temperatures between 23 and 1000°C; although they found no visual microstructural change, material cation exchange capacity (CEC) dropped significantly above 300°C, indicating a loss of chemically bound water and the onset of clay particle rearrangement due to the exposure of charged particle surfaces. The dark colour may be due to the formation of a reducing environment as a consequence of rapid heating (Akinshipe and Kornelius, 2017).

### Thermal Property Modelling

Figure 7 shows the modelled performance against measured data for selected specimens tested at each heat flux. Estimated thermal properties are given in Table 2 (note that two specimens were not modelled – one at 25 kW/m<sup>2</sup> and one at 50 kW/m<sup>2</sup> – due to insufficient data). By means of comparison, thermal properties for common construction materials are given in

Table 3.

The results of the modelling were mixed with respect to capturing behaviour recorded in the tests. The overall shape of the temperature time curve above 100°C for each thermocouple was replicated. However, the ‘plateau’ at 100°C, although present as a change in the slope of the heating rate, was not as pronounced in terms of its consistency of temperature (i.e. remaining at 100°C) or its duration as was observed during the tests, most notably for higher heat fluxes. Further investigation is required to establish the exact source of this discrepancy. However, there are several possible sources. Since the plateau is associated to the latent heat of water, it is possible that a heat transfer model (even with the use of an apparent specific heat capacity) is

insufficient to capture the behaviour of the moisture within the sample. It is possible

Table 2. Finite difference model thermal properties (parameter subscripts as per Figure 4)

Heat flux [kW/m <sup>2</sup> ]	$k_1$ [W/mK]	$k_2$ [W/mK]	$\rho_1$ [kg/m <sup>3</sup> ]	$\rho_2$ [kg/m <sup>3</sup> ]	$c_p$ [J/kgK]	$c_{p,max}$ [J/kgK]
25	2.00	0.62	2132	2033	755	4188
25	1.81	0.69	2145	2045	872	5557
35	2.00	0.57	2142	2074	750	2528
35	2.00	0.61	2144	2076	751	4649
35	1.78	0.55	2046	1987	886	5927
50	1.89	0.69	2157	2079	826	5411
50	1.98	0.51	2064	2015	772	5647

Table 3. Typical thermal property values for common building materials (Drysdale, 2011)

Material	$k$ [W/mK]	$c_p$ [J/kgK]	$\rho$ [kg/m <sup>3</sup> ]
Brick	0.69	840	1600
Concrete	0.8-1.4	880	1900-2300
Gypsum plaster	0.48	840	1440

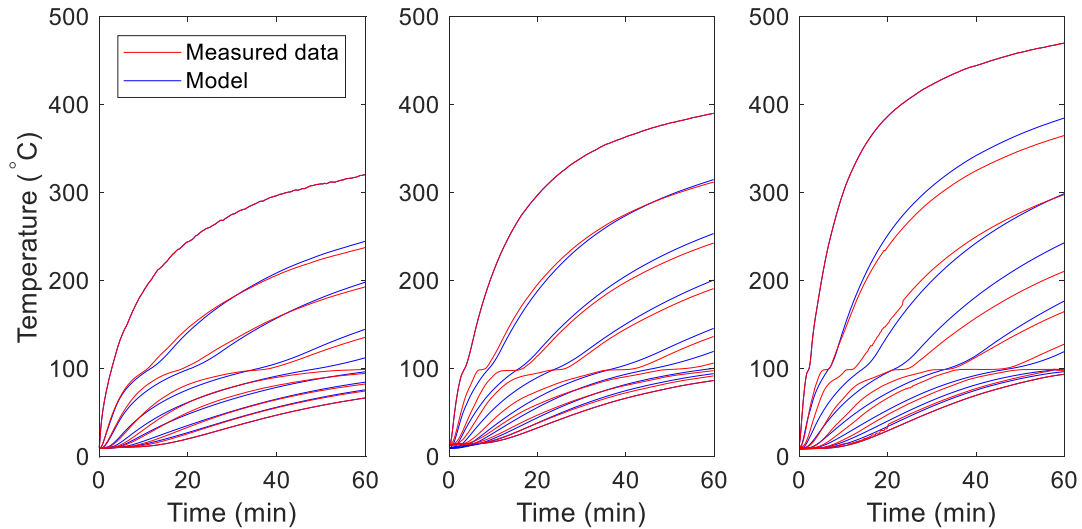


Figure 7. Comparison of modelled performance against measured data at 20, 35 and 50 kW/m<sup>2</sup> (left to right respectively).

that moisture migration may occur as water moves further into the samples and condenses, due to the high thermal gradient; this would have the overall impact of accelerating the transfer of energy ahead of the thermal wave and potentially prolonging the time at which each part of the material was maintained at 100°C. A heat and mass transfer model would therefore be required to capture this behaviour. It is worth noting, however, that the impact of the moisture appears to be greater than in concrete modelling, for which the apparent thermal property modelling approach is commonly used and is capable of reproducing observed thermal changes without needing to account for moisture migration. This further raises the question of whether this is due to the internal structure of rammed earth and the ease with which moisture is able to migrate through the material.

Irrespective of the limitations discussed above, modelled data suggests that conductivity is likely to be lower once the material has been dried and heated:  $k_1$  was significantly higher than  $k_2$  for all specimens. This agrees with Hall and Allinson's findings, however the lower bound (roughly 0.6 W/mK) is low compared to the literature results for a dry earthen material (roughly 0.9 W/mK). Notably, 0.6 W/mK is close to the thermal conductivity of fired brick (

Table 3), intimating that thermo-chemical processes occurring in the rammed earth as it is heated make it behave much like fired brick after the removal of water.

Specific heat capacity values fell within the lower part of the range that was specified – between 750 and 890 J/kgK – and were, again, close to values found by Hall and Allinson and similar to values associated with fired brick and concrete. It is emphasized here that the higher values found for  $c_{p,max}$  are features of the modelling procedure and do not represent real properties.

Given the variability of these results, and the degree to which moisture appears to have played a dominant role in the heating of the sample, it is recommended that further work be undertaken to verify these values. Nevertheless, these results lend support to a heat transfer method to estimate thermal properties and give an indication of the likely trends – particularly with respect to conductivity as a function of temperature.

## CONCLUSION

This paper has presented results for heating unstabilised rammed earth specimens under constant heat flux and a method to predict material thermal properties by means of a heat transfer finite difference model. Temperatures measured nearest to and furthest from the heat source defined the thermal boundary conditions and an apparent thermal property approach was used to accommodate the phase change of liquid water trapped within the pore space for heating above 100°C.

Testing revealed that specimens remained intact during and after heating. The heated surface displayed a reddening effect, associated with the oxidation of metal cations within the material structure, over a depth of roughly 5 mm, overlying a darkened layer of roughly 10 mm depth. Darkening was suggestibly due to the dehydration of chemically bound water in a reducing environment. However, additional testing is required to examine the exact nature of the presumed oxidised and dehydrated material.

The model provided a better match to temperature changes observed above 100°C than those found at and below. Predicted thermal properties were similar to those found in the literature for either rammed earth materials (tested below 100°C) or fired brick, indicating that the heated rammed earth specimens transitioned between these two conditions. However, the predicted plateau in temperature readings, due to water evaporation, was less pronounced than in measured results. It was proposed that this was due to moisture migration under the extreme heat gradient, so that a combined heat-mass-transfer model would be required, rather than the solely heat transfer model employed here. Additional moisture content data is required to examine this more fully.

## ACKNOWLEDGEMENTS

The authors would like to thank the technical staff at the University of Edinburgh's School of Engineering for assisting in the preparation of the sample moulds and drill attachments.

## REFERENCES

- Adam, E. A. & Jones, P. J. (1995). "Thermophysical properties of stabilised soil building blocks". *Building and Environment*, 30 (2), 245-253
- Akinshipe, O. & Kornelius, G. (2017). "Chemical and thermodynamic processes in clay brick firing technologies and associated atmospheric emissions metrics -- A review". *Journal of Pollution Effects & Control*, 5 (2), 1000190-1-12
- Arrigoni, A., Grillet, A.-C., Pelosato, R., Dotelli, G., Beckett, C. T. S. & Ciancio, D. (2017). "Reduction of rammed earth's hygroscopic performance under stabilisation: an experimental investigation". *Building and Environment*, 115, 358-367
- Beckett, C. T. S. & Augarde, C. E. (2013). "Prediction of soil water retention properties using pore-size distribution and porosity". *Canadian Geotechnical Journal*, 50 (4), 435-450
- Beckett, C. T. S. & Ciancio, D. (2014). "Effect of microstructure on heat transfer through compacted cement-stabilised soils". Soga, K., Kumar, K., Biscontin, G. & Kuo, M. (Eds.). *Geomechanics from Micro to Macro*, CRC Press, 2, 1539-1544
- Beckett, C. T. S., Augarde, C. E., Easton, D. & Easton, T. (2018). "Strength characterisation of soil-based construction materials". *Géotechnique*, 65 (5), 400-409
- British Standards. "BS 1377-4:1990. Methods of testing for soils for civil engineering purposes – Part 4: Compaction-related tests". British Standards Institution
- British Standards. "BS EN 1992-1-2:2004 Design of concrete structures - Part 1-2 General rules - Structural fire design". British Standards Institution
- Drysdale, D. (2011). "An introduction to fire dynamics". John Wiley and Sons Ltd, UK
- Gens, A. (1997). "Suction and temperature, critical factors affecting soil behaviour". *Proc. 14th Int. Conf. Soil Mech. Found. Engng*, 4, 2169-2171

- Gens, A. (2010). "Soil-environment interactions in geotechnical engineering". *Géotechnique*, 60 (1), 3-74
- Goodman, C. C., Latifi, N. & Vahedifard, F. Stuedlein, A. W., Lemnitzer, A. & Suleiman, M. T. (Eds.) (2018). "Effects of temperature on microstructural properties of unsaturated clay". *Advances in Geomaterial Modeling and Site Characterization*, 343-352
- Hall, M. & Djerbib, Y. (2004). "Rammed earth sample production: context, recommendations and consistency". *Construction and Building Materials*, 18 (4), 281-286
- Hall, M. & Allinson, D. (2009). "Analysis of the hygrothermal functional properties of stabilised rammed earth materials". *Building and Environment*, 44 (9), 1935-1942
- Hidalgo, J. P. (2015). "Performance-based methodology for the fire safe design of insulation materials in energy efficient buildings". School of Engineering, The University of Edinburgh
- Houben, H. & Guillaud, H. (1994). "Earthen architecture: A comprehensive guide". Intermediate Technology Development Group, London (UK),
- Jaquin, P. A., Augarde, C. E., Gallipoli, D. & Toll, D. G. (2009). "The strength of unstabilised rammed earth materials". *Géotechnique*, 59 (5), 487-490
- Johari, I., Said, S., Hisham, B., Bakar, A. & Ahmad, Z. A. (2010). "Effect of the change of firing temperature on microstructure and physical properties of clay bricks from Beruas (Malaysia)". *Science of Sintering*, 245-254
- Mielenz, R. C., Schieltz, N. C. & King, M. E. (1953). "Thermogravimetric analysis of clay and clay-like minerals". *Clays and Clay Minerals*, 2, 285-314
- Smith, J. C. & Augarde, C. E. (2014). "Optimum water content tests for earthen construction materials". *Construction Materials*, 167 (2), 114-123
- Zhou, A., Huang, R.-Q. & Sheng, D. (2016). "Capillary water retention curve and shear strength of unsaturated soils". *Canadian Geotechnical Journal*, 53(6), 974-987